

# Antioxidant biocompatible composite collagen dressing for diabetic wound healing in rat model

Bei Qian<sup>1,2,†</sup>, Jialun Li<sup>1,2,†</sup>, Ke Guo<sup>1,2</sup>, Nengqiang Guo<sup>1,2</sup>, Aimei Zhong<sup>1,2</sup>, Jie Yang<sup>1,2</sup>, Jiecong Wang<sup>1,2</sup>, Peng Xiao<sup>1,2</sup>, Jiaming Sun<sup>1,2,\*</sup> and Lingyun Xiong<sup>1,2,\*</sup>

<sup>1</sup>Department of Plastic Surgery, Union Hospital, Tongji Medical College, Huazhong University of Science and Technology, 1277 Jiefang Avenue, Wuhan 430022, China; <sup>2</sup>Wuhan Clinical Research Center for Superficial Organ Reconstruction, Wuhan 430022, China

\*Correspondence address. Department of Plastic Surgery, Union Hospital, Tongji Medical College, Huazhong University of Science and Technology, 1277 Jiefang Avenue, Wuhan 430022, China. Tel: 027-85726114; Fax: +86-21-58702208; E-mail: 2004xh0801@hust.edu.cn (J.S.); xionglyingyun1986@163.com (L.X.)

<sup>†</sup>These authors contributed equally to this work.

Received 5 November 2020; revised 29 December 2020; accepted on 4 January 2021

## Abstract

Associated with persistent oxidative stress, altered inflammatory responses, poor angiogenesis and epithelization, wound healing in diabetic patients is impaired. N-acetylcysteine (NAC) is reported to resist excess reactive oxygen species (ROS) production, prompt angiogenesis and maturation of the epidermis. Studies have revealed that graphene oxide (GO) can regulate cellular behavior and form cross-links with naturally biodegradable polymers such as collagen (COL) to construct composite scaffolds. Here, we reported a COL-based implantable scaffold containing a mixture of GO capable of the sustained delivery of NAC to evaluate the wound healing in diabetic rats. The morphological, physical characteristics, biocompatibility and NAC release profile of the GO-COL-NAC (GCN) scaffold were evaluated *in vitro*. Wound healing studies were performed on a 20 mm dorsal full-skin defect of streptozotocin (STZ)-induced diabetic rats. The injured skin tissue was removed at the 18th day post-surgery for histological analysis and determination of glutathione peroxidase (GPx), catalase (CAT) and superoxide dismutase (SOD) activity. In diabetic rats, we confirmed that the GCN scaffold presented a beneficial effect in enhancing the wound healing process. Additionally, due to the sustained release of NAC, the scaffold may potentially induce the antioxidant defense system, upregulating the expression levels of the antioxidant enzymes in the wound tissue. The findings revealed that the antioxidant biocompatible composite collagen dressing could not only deliver NAC *in situ* for ROS inhibition but also promote the wound healing process. This scaffold with valuable therapy potential might enrich the approaches for surgeon in diabetic wound treatment in the future.

**Keywords:** collagen; graphene oxide; N-acetylcysteine; sustained release; diabetic wound healing

## Introduction

Diabetes mellitus (DM) is a chronic metabolic disorder, affecting more than 340 million people, with nearly 20% of them developing diabetic wounds globally [1]. Based on a previous report, in every

30 s, one leg is amputated as a result of impaired wound healing in diabetic patients worldwide [2]. Owing to the absence of measures for prevention, non-healing and poorly healing wounds pose a serious global health threat with elevated DM prevalence [3]. The

critical cause of the poor healing of the diabetic wound is prolonged inflammation, poor vascularization and epithelization, and deficient collagen deposition [4]. Additionally, the sustained reactive oxygen species (ROS) production would further delay the recovery of wounds in diabetic patients [3, 5]. Thus, the wound dressing biomaterials with the ability to promote diabetic wound healing have been widely studied.

The biomaterials currently used as matrices for wound repair can be classified into natural and synthetic types according to their origin [6]. Due to the characteristics of easy degradation, remarkable biocompatibility, reduced inflammatory responses and non-immunogenic nature, natural biomaterial has been widely recommended, such as collagen (COL) [7]. COL, one of the main extracellular matrix (ECM) protein factors, potentially regulates the cell phenotype and is involved in the modification of physicochemical characteristics of the scaffold [8]. Moreover, benefits from the chemical groups, abundant in the branches of the molecular structure, COL is reported to be the vehicle cross-linked multiple drugs [9]. Unfortunately, poor mechanical properties, the unstable porous structure under wet conditions, and lack of biological activity limit the application of pure COL scaffolds [10].

Graphene oxide (GO), a highly oxidized form of graphene, in which the quasi-two-dimensional (2D) spatial structure of carbon atoms is decorated with oxygen-containing functionalities [11]. Numerous oxygen-functional groups, including carboxylic, epoxy and hydroxyl groups make its surface open for covalent, electrostatic and hydrogen bonding with biomolecules and therapeutic drug, which endows drugs with targeted and sustained features, and improves the biocompatibility of GO [12]. Studies have reported that GO has the potential to promote cellular proliferation, differentiation and adhesion with no or little cytotoxic effect [13, 14].

Moreover, the inclusion of GO nanosheets can substantially improve the mechanical strength to GO-related polymeric scaffolds [15]. After implantation into the body, scaffolds with GO are degraded via peroxidase secreted by immune cells; eventually, their excretion occurs in the form of feces and urine [16]. Thus, owing to its remarkable biocompatibility, biodegradation and mechanical properties, polymeric scaffolds incorporated with GO hold great potential for tissue engineering applications [17].

N-acetylcysteine (NAC) is a transformed version of cysteine (amino acid), which can permeate cell membrane and rapidly hydrolyze to give cysteine, a precursor of glutathione (GSH). By restoring the intracellular natural antioxidant glutathione levels, NAC assists the cells in eliminating the damaging impacts of the ROS along with a high safety profile [18]. As an antioxidant, NAC has been receiving growing research attention in promoting wound healing [19]. Recently, Ozkaya *et al.* [20] reported using a diabetic rat model that NAC improved healing of wounds by reducing the oxidative stress parameters in both tissue and serum. Zayed and colleagues [21] found that NAC accelerated amputation stump healing not only through resisting oxidative stress of the wound but also by promoting vascularization. There are also reports that NAC promotes the expression of matrix metalloproteinase 1 (MMP-1) through the PKC/Stat3 signaling pathway, thereby promoting epidermal maturation [22]. Besides, the carboxyl group of NAC has been confirmed to be chemically cross-linked to the amino group or hydroxyl group, thereby achieving sustained release of NAC [23]. This would ensure adequate drug concentration on the wound, especially in cases of prolonged healing.

Herein, a novel N-acetylcysteine-controlled-release graphene oxide-collagen scaffold (GO-COL-NAC) was developed with 2 mm

height and 20 mm diameter, which cross-linked by the carbonized diimine (EDC) and n-hydroxy succinimide (NHS) systems. The surface morphological features of the hybrid scaffolds were assessed using scanning electron microscopy (SEM). To characterize the scaffolds, we used Fourier transform infrared (FTIR), X-ray diffraction (XRD), Raman spectroscopy and spectroscopy. The physical properties, biocompatibility of this scaffold and its ability to release drugs sustained were assessed *in vitro*. Then, the constructed scaffolds were implanted into a rat model having a skin defect (20 mm full-thickness) on the dorsal side, to evaluate the GO-COL-NAC (GCN) scaffold effect on wound healing in the streptozotocin-induced diabetic rats.

## Materials and methods

### Preparing GO-COL and GO-COL-NAC composite scaffolds

Firstly, type I COL (Sigma-Aldrich, America) was cut into pieces, dissolved in acetic acid (0.05 M) to generate a 2% (w/v) suspension. Secondly, upon dissolving GO (Sigma-Aldrich, USA) in distilled water, we sonicated the solution for 30 min using an ultrasonic processor (Branson, USA) to generate a 0.2% (w/v) solution. Thirdly, the GO solution was mixed with COL suspension completely in a 1:5 volume ratio and added NAC (Sigma-Aldrich, USA) (500 mg/L) aqueous solution. The obtained mixture was then sonicated at 70% intensity in an ice bath for 60 min to obtain a homogeneous state. Fourthly, the mixed solution was filled into a pre-designed cylindrical model (20 mm, diameter; 2 mm, height). We then froze the solution at  $-20^{\circ}\text{C}$  overnight. This was followed by a 24 h lyophilization at  $-50^{\circ}\text{C}$ , after which we obtained a porous scaffold. Finally, we cross-linked the scaffolds chemically through immersion into EDC (50 mM) (Sigma-Aldrich, USA) with NHS (20 mM) (Sigma-Aldrich, USA) solution ( $\text{H}_2\text{O}/\text{ethanol} = 5:95$ ) for 24 h, adequately washed using distilled water, then freeze-dried at  $-50^{\circ}\text{C}$ ; resulting in a cross-linked GO-COL-NAC composite scaffold (Fig. 1A). We fabricated the control GC, GCN100 mg/L and GCN1000 mg/L scaffolds through the same methods, but the added NAC concentration was 0, 100 mg/L and 1000 mg/L, respectively.

### Characterizing GO-COL and GO-COL-NAC composite scaffolds

#### Morphology of GO-COL and GO-COL-NAC composite scaffolds

The SEM (JSM-IT300, JEOL, Tokyo, Japan) run at a high voltage (20 kV) was used to characterize the morphology of the GO-COL and GO-COL-NAC scaffold specimens after sputter-coating them with gold-palladium.

### Water absorption rate, water retention ratio and porosity

The water absorption rate and retention rate of the scaffolds were measured as reported previously [24]. Briefly, dry scaffolds were weighed ( $W_1$ ), immersed in distilled water at room temperature for 24 h. Using a filter paper, the surface water was absorbed, and the wet weight was designated as  $W_2$ . Upon filling the scaffolds with water, the tubes were centrifuged (500 rpm, 3 min) then re-weighed ( $W_3$ ). To calculate the percentage weight absorption and retention rate of the GO-COL or GO-COL-NAC scaffold, we utilized the following equation.

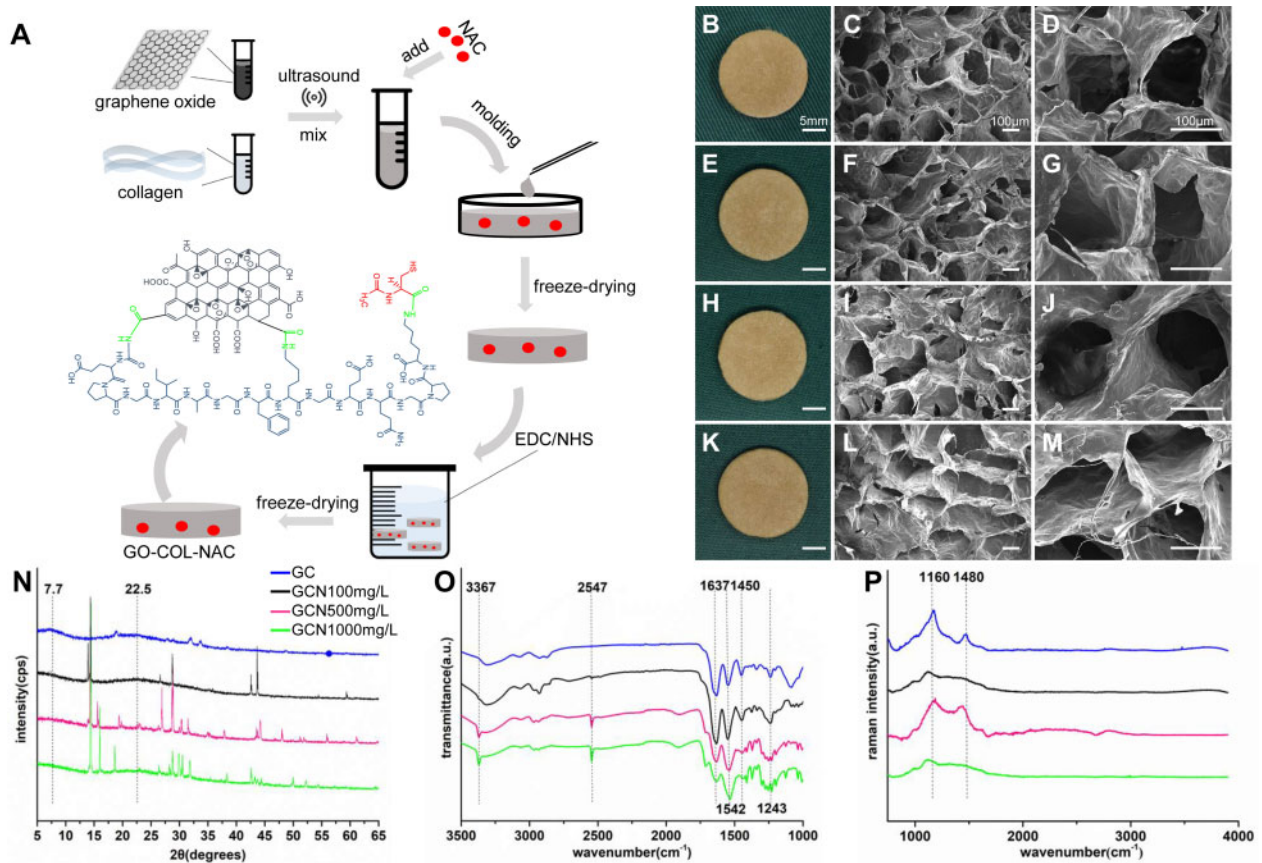


**Figure 1.** Characterizations of engineered hybrid scaffolds. (A) Schematic illustration showing how GO-COL-NAC scaffolds were prepared. GO and COL were dissolved, adequately under an ultrasonic wave. Add the NAC and mix again, the mixture was filled into molds to generate GO-COL-NAC scaffolds with cylindrical shape with 20 mm diameter and 2 mm height. After freeze-dried, cross-linked by EDC/NHS and freeze-dried again, the GO-COL-NAC scaffolds were prepared. Macroscopic view and SEM images of the GO-COL (B, C-D), GO-COL-NAC100 mg/L (E, F-G), GO-COL-NAC500 mg/L (H, I-J) and GO-COL-NAC1000 mg/L (K, L-M). (N) X-ray diffractometer, (O) Fourier infrared spectrometer, black dashed line in 2547  $\text{cm}^{-1}$  indicates the characteristic peak of NAC and (P) Raman spectroscopy, dashed lines in 1160 nm and 1480 nm show the specific peak of GO

$$\text{Water absorption rate (\%)} = [(W_2 - W_1)/W_1] * 100\%$$

$$\text{Water retention rate (\%)} = [(W_3 - W_1)/W_1] * 100\%$$

The porosity of the scaffolds was determined according to the modified liquid displacement method reported in the previous study [25]. Firstly, the following measurements were taken: the radius ( $r$ ), thickness ( $b$ ), and dry weight ( $W_d$ ) of the scaffold. Secondly, the scaffold was immersed into absolute ethanol for 24 h at room temperature, then taken out and immediately weighted as  $W_w$ . Each of the above values was given based on the average of three parallel specimen measurements. The following formula was used to calculate the porosity of the GO-COL or GO-COL-NAC scaffold:

$$\text{Porosity (\%)} = [(W_w - W_d)/(\rho b \pi r^2)] * 100\%$$

where  $\rho$  represents the absolute ethanol density ( $0.789 \text{ g/cm}^3$ ), and the  $\pi$  value is 3.14159.

#### X-ray diffraction, Raman spectra analysis and Fourier transform infrared spectroscopy

X-ray diffraction (XRD, Empyrean, PANalytical B.V. Netherlands) with  $\text{Cu K}\alpha$  radiation (scanning rate:  $1.4583^\circ/\text{s}$ ,  $2\theta$  range from  $5^\circ$  to  $65^\circ$ ) was used to evaluate the crystalline phases of the scaffolds. Raman microscope (Rfs 27 FT, Bruker, Germany) was applied to

examine the composition of the scaffolds; the scanning range was  $50\text{--}4000 \text{ cm}^{-1}$  at room temperature. The excitation source is a diode laser with wavelength ( $532 \text{ nm}$ ) and power ( $30 \text{ mW}$ ) [26]. Functional groups of the scaffolds were confirmed using Fourier transform infrared spectroscopy (FTIR, VERTEX 70, Bruker, German) ( $4000\text{--}500 \text{ cm}^{-1}$ ) with  $2 \text{ cm}^{-1}$  resolution.

#### The release kinetics of NAC in GO-COL-NAC scaffolds

The drug release properties of the scaffolds were using high-performance liquid chromatography (HPLC, Agilent, USA) using a C18 chromatographic column measuring  $200 \text{ mm} \times 4.6 \text{ mm}$ ,  $5 \mu\text{m}$ . The mobile phase contained  $20 \text{ mmol/L}$  sodium dihydrogen phosphate solution (adjusted pH to 2.5 with 50% phosphoric acid)-acetonitrile (v/v, 94:6) run at a flow rate of  $1.0 \text{ ml/min}$ . The injection volume was  $10 \mu\text{L}$ , and  $210 \text{ nm}$  was set as the detection wavelength. Firstly, NAC solutions with different standard concentrations were prepared with a phosphate-buffered solution (PBS). The characteristic peak of NAC was detected by HPLC, and the peak height of the characteristic peaks at different concentrations was recorded. Then a simple unary linear regression between the standard concentration and peak height was established. Secondly, the GO-COL-NAC scaffold was immersed in  $2 \text{ ml}$  PBS at  $37^\circ\text{C}$  with shaking at  $60 \text{ rpm}$ . The supernatants were collected from the scaffold following centrifugation at  $3000 \text{ rpm}$  for  $5 \text{ min}$  at each scheduled time-points

(6 h, 12 h, 1 day, 3 days, 7 days, 14 days, 18 days), respectively, and subsequently detected by HPLC. The released NAC was calculated according to the acquired unary function. The experiments were performed in triplicate.

### *In vitro* cell biocompatibility of the GO-COL and GO-COL-NAC scaffolds

NIH 3T3 fibroblasts (ATCC, USA) were used for cell proliferation assay and HaCaT cells (ATCC, USA) for cell migration assay. The cells were maintained in growth media (GM) enriched with Dulbecco's modified Eagle's medium (DMEM, Thermo Fisher Scientific, USA) High glucose containing fetal bovine serum, 10% (FBS, Thermo Fisher Scientific, USA), and penicillin/streptomycin, 1% (Thermo Fisher Scientific, USA) at 37°C and 5% CO<sub>2</sub> in a humidified incubator. For cell detachment, we used 0.05% trypsin, but replaced the media every 2 days.

The scaffolds sterilized using ethylene oxide gas were immersed in the DMEM high glucose medium for 24 h. Subsequently, we collected the media, centrifuged for 5 min at 1000 rpm, then filtered them through a 0.20 μm syringe filter. The filtered media as the extract liquor of the scaffold were collected for cytology experiments [27].

### *In vitro* cell proliferation assay

The cell proliferation assay was used to estimate the cytotoxicity of the scaffold according to the protocol previously described [28]. The NIH-3T3 fibroblasts were cultured up to confluency and seeded in a 24-well plate 2 × 10<sup>4</sup> cells/well followed by incubation for 24 h. Subsequently, the medium in the 24-well plate was respectively replaced with four different extract liquors, low glucose medium and high glucose medium in six groups. The plate was subjected to the IncuCyte S3 Live-Cell Analysis System (Essen Bioscience) where real-time images were captured every 8 h. The proliferation phase was assessed using IncuCyte S3 Software (Essen Bioscience) and compared between groups.

### Real-time polymerase chain reaction analysis for collagen

The mRNA expression levels of COL Type I and COL Type III of the NIH-3T3 fibroblasts in different extract liquor were measured using real-time polymerase chain reaction (RT-PCR). Total RNA extraction from the cultured NIH-3T3 fibroblasts was performed using Trizol reagent (Thermo Fisher Scientific, USA) and reverse-transcribed using the Revert Aid First Strand cDNA Synthesis Kit (Thermo Fisher Scientific, USA). The primer sequences used are shown in supporting information, as in [Supplementary Table S1](#). For RT-PCR, we used using AceQ Universal SYBR qPCR Master Mix (Vazyme Biotech Co., Ltd) on a real-time PCR system (Stepone plus, ABI, USA) for PCR product quantification. Amplification conditions were as follows: 95°C for 5 min, 95°C for 10 s, and 60°C for 30 s (40 cycles). mRNA expression level in all experimental groups was determined using the 2<sup>-ΔΔCT</sup> method.

### *In vitro* cell migration (scratch) assay

The keratinocyte migration assay was conducted for *in vitro* evaluation of re-epithelialization. HaCaT cells were seeded in 24-well plates with a density of 2.5 × 10<sup>5</sup> cells in each well and cultured to form a confluent monolayer. Next, add the mitomycin with a concentration of 10 μg/ml and incubate for 3 h. Scratch wounds were created on the cell monolayers using a 200 μL pipette tip and

rinsed with PBS gently. Thereafter, with a different extract liquor, we substituted the medium in each well. At 4 h, 8 h, 12 h, 16 h and 24 h of incubation, the cells were subjected to PBS wash, after which images of the scratched wounds were taken. Measurement of the area of the remaining scratched wound at each time-point was taken using Image J software. The setting of the control group is the same as the cell proliferation assay.

### *In vivo* wound healing studies

Study protocols were approved by the Animal Ethical Committee of Huazhong University of Science and Technology (HUST; all animals were obtained from the Laboratory Animal Center of HUST).

Sixteen male 6-weeks-old Sprague–Dawley (SD) rats, with an average weight of 180–200 g were maintained adaptively in a room with controlled humidity and temperature for one week. After fasting overnight, we injected all rats with streptozotocin (STZ, Sigma-Aldrich, USA, 50 mg per kg body weight) in the right upper abdomen. The SD rats with the fasting glucose level > 11.1 mmol/L for three consecutive days were considered DM. Otherwise, STZ was injected again until the DM model was successfully constructed.

To anesthetize the 8 diabetic rats, 10% chloral hydrate (Sigma-Aldrich, USA, 0.4 ml per 100 g) was used via intraperitoneal injection, and their dorsal hairs were shaved. The incision was marked with methylene blue and subsequently disinfected with iodophor. Five full-thickness wounds (20 mm diameter) was randomly created at either side of the dorsal central line in experimental animals. Wounds in each rat were treated with the following: the blank control, GC, GCN100 mg/L, GCN500 mg/L and GCN1000 mg/L randomly; then the wound area was fixed with a medical bandage. The bandage was changed every two days. Using a Canon digital camera, wound images were recorded at days 0, 3, 7, 14 and 18 post-surgery. Image J software was used to quantify the surface area of the wound at each time-point. Then, to calculate the rate of wound closure, we used the following formula:

$$\text{Wound closure rate} = (S_0 - S_x) / S_0 * 100\%$$

Where S<sub>0</sub> refers to the original wound area and S<sub>x</sub> denotes the area of the wound at days 0, 3, 7, 14 and 18 post-surgery.

### Histological analysis

All the experimental rats were sacrificed at day 18 post-surgery, and tissues including both unwounded and wounded areas were collected and then fixed in 10% formaldehyde. Hematoxylin–Eosin (H&E) and Masson trichrome stains (Sigma-Aldrich, USA) of wound tissue 18 days post-surgery were performed separately to evaluate the epidermis, collagen and new tissue generation. Similarly, the immunohistochemical stain with antibodies against human-specific CD31 (Sigma-Aldrich, USA) was implemented to observe the vascular endothelial cells [29]. An optical microscope (Nikon H600L, Tokyo, Japan) was used to examine the cells and take images.

### Detection of antioxidant stress level

The relative mRNA expression of various antioxidant kinases, including catalase (CAT), superoxide dismutase (SOD) and glutathione peroxidase (GPx) in skin wound skin samples was determined by RT-PCR analysis according to the protocol described above. The following amplification conditions were used: 95°C for 5 min, 95°C for 10 s and 60°C for 30 s (40 cycles). A list of primers used for PCR is provided in [Supplementary Table S2](#).

## Statistical analysis

We presented all data from the repeated experiments as the mean  $\pm$  standard deviation, then assessed using Tukey's *t*-tests and one-way ANOVA (SPSS software, USA; GraphPad Prism, USA). The significance levels were denoted as follows: \*, \*\*, and \*\*\*, referring to the *P* values of <0.05, <0.01 and <0.001, respectively.

## Results

### Preparation and characterization of GO-COL and GO-COL-NAC scaffolds

The cylindrical GO-COL and GO-COL-NAC scaffolds with a diameter of 20 mm and a height of 2 mm were successfully prepared after crosslinking and re-lyophilizing procedures. As depicted in Fig. 1B, E, H, K, various scaffolds prepared showed the same appearance of a brown sponge. SEM micrographs displayed that the morphologies of GO-COL and GO-COL-NAC scaffolds were both highly interconnected porous under different magnifications (Fig. 1C–D, F–G, I–J, L–M).

The quantitative results of the water absorption rate, water retention rate and porosity about the scaffolds were presented in Supplementary Table S3, which exerted a crucial role in the cell in-growth and metabolite [30]. No significant difference was found between the three parameters of each group, indicating that the similarity in physiochemical properties, and the concentration of NAC has no effect on the structure of the scaffold.

Figure 1N shows the XRD analysis of each sample. When  $2\theta = 22.5^\circ$  and  $7.7^\circ$ , the broad diffuse peak was presented, which could be attributed to the homogeneous COL and GO, respectively. However, the characteristic narrow diffraction peak seen on the NAC-loaded samples may represent the NAC in the form of a microcrystal phase.

The Functional groups of the scaffolds were confirmed by FTIR (Fig. 1O). The appearances of amide I (C=O stretch) around  $1637\text{ cm}^{-1}$ , amide II (N–H stretch) around  $1542\text{ cm}^{-1}$ , and amide III (C–N stretch) around  $1450\text{ cm}^{-1}$ , were dedicated to the COL bands in all four groups [9]. Meanwhile, the characteristic peaks of the GO at  $3367\text{ cm}^{-1}$  were observed [31]. The C–O–C stretching corresponded to the peak around  $1233\text{ cm}^{-1}$ , and the sulfhydryl group (–SH) stretching (at  $2547\text{ cm}^{-1}$ ) was specifically seen in all NAC-loaded samples [26].

Using the Raman spectrum (Fig. 1P), the carbon components were revealed in the four scaffold groups. Notably, four sample groups presented the characteristic 'M' peak composed of D band (around  $1160\text{ cm}^{-1}$ ) and G band (around  $1480\text{ cm}^{-1}$ ) (Fig. 1P), which was emitted by the vibration of sp<sup>2</sup> hybridized carbon atom plane, indicating the existence of GO in the composite scaffolds.

### The release kinetics of NAC in GO-COL-NAC scaffolds

Here, we have presented the release profiles for the GO-COL-NAC scaffolds in Fig. 5C, demonstrating that the NAC loaded in the scaffolds could be persistently released for at least 18 days. The curves of the three groups were basically identical, containing two stages. The NAC was released rapidly in the first 24 h, about  $51.96 \pm 1.35\%$  ( $51.9 \pm 1.35\ \mu\text{g}$ ) of the total loaded drug in the GCN100 mg/L,  $49.42 \pm 0.35\%$  ( $247.1 \pm 1.75\ \mu\text{g}$ ) in GCN500 mg/L and  $49.74 \pm 1.63\%$  ( $497.4 \pm 16.3\ \mu\text{g}$ ) in GCN1000 mg/L groups. Between 24 h and 14 days, the release rate slowed down, obviously. The cumulative released drug percentage of the GCN100 mg/L was about  $72.89 \pm 0.75\%$ , the GCN500 mg/L was  $72.77 \pm 0.50\%$ ; the

GCN1000 mg/L was  $71.05 \pm 0.86\%$ . The average released dosage of the three groups in the last 4 days was  $3.23 \pm 0.52\ \mu\text{g}$ ,  $12.85 \pm 1.07\ \mu\text{g}$  and  $29.24 \pm 3.58\ \mu\text{g}$ , respectively.

### *In vitro* cell biocompatibility of the GO-COL and GO-COL-NAC scaffolds

Cell proliferation of the NIH-3T3 fibroblasts was shown in Fig. 2A. It could be observed that there were more cells in all groups upon increasing culture time for 80 h post-seeding, which suggested the scaffolds had no obvious cytotoxicity. While the GCN500 mg/L group and the negative control group (low glucose) exhibited higher living cell density at 80 h, confirming the better cell proliferation viability compared to the other groups. Some cells in the positive control group (high glucose) had lost their bioactivity, and cells in other groups remain active, although the density of the living cells was relatively low. The NIH-3T3 fibroblasts proliferation phase (Fig. 2B) of the GCN500 mg/L group and the negative control group reached  $95.44 \pm 1.0\%$  and  $96\% \pm 1.45\%$  respectively, remarkably higher compared to the other groups; notably, the difference exhibited statistical significance ( $P < 0.01$ ).

The RT-PCR was performed to detect the COL gene expression of NIH-3T3 fibroblasts in the extract liquor of scaffolds. Results (Fig. 6A and B) indicated that the GCN500 mg/L group showed a significantly higher gene expression of the COL Type I ( $1.81 \pm 0.05$  fold) and COL Type III ( $1.95 \pm 0.06$  fold) compared with other groups.

These outcomes demonstrated that the scaffolds had good biocompatibility and had a better ability to improve COL secretion potential of fibroblasts in a high-glucose environment when NAC concentration was 500 mg/L ( $P < 0.05$ ).

The result of the keratinocyte migration (scratch) assay *in vitro* was shown in Fig. 2C and D. Since keratinocytes were the main cell types that contributed to the wound healing, this general cell migration trend (Fig. 2C) partly reflected the potential of the scaffolds to re-epithelialize *in vitro* [27]. The quantitative analysis (Fig. 2D) using the Image J and Graphpad Software revealed that the HaCaT cell migration rate of each group at 24 h were  $42.83 \pm 4.36\%$  (GC group),  $50.01 \pm 3.99\%$  (GCN100 mg/L group),  $58.17 \pm 3.67\%$  (GCN500 mg/L group),  $52.08 \pm 2.23\%$  (GCN1000 mg/L group),  $64.73 \pm 3.66\%$  (low glucose group, negative control),  $36.91 \pm 4.68\%$  (high glucose group, positive control), respectively. Obviously, the GCN500 mg/L group had a faster cell migration rate in the experimental group ( $P < 0.05$ ), only slightly slower than that of the negative control group ( $P > 0.05$ ).

### *In vivo* wound healing studies

There was a certain mortality rate in the process of diabetic modeling (2 deaths per 10 rats), and an increase in blood sugar, and a decrease in STZ-injected rat's weight. Finally, eight rats with fasting blood glucose greater than  $11.1\text{ mmol/L}$  for three consecutive days were included *in vivo* experiment. Five full-thickness wounds (20 mm diameter) were created at in each diabetic rat to compare the wound healing efficiency between four scaffolds and one blank control, and Fig. 3A was the schematic of the experiment. Fig. 3B shows the macroscopic images of the dorsal wounds at days 0, 3, 7, 14 and 18 post-surgery. In the first 7 days, all the scaffolds adhered well on the wound surface, and there seemed to be no significant difference in the healing rates of all wounds. Subsequently, the scaffolds were degraded subcutaneously, and the wound area of each group showed a large difference. The quantitative analysis shown in

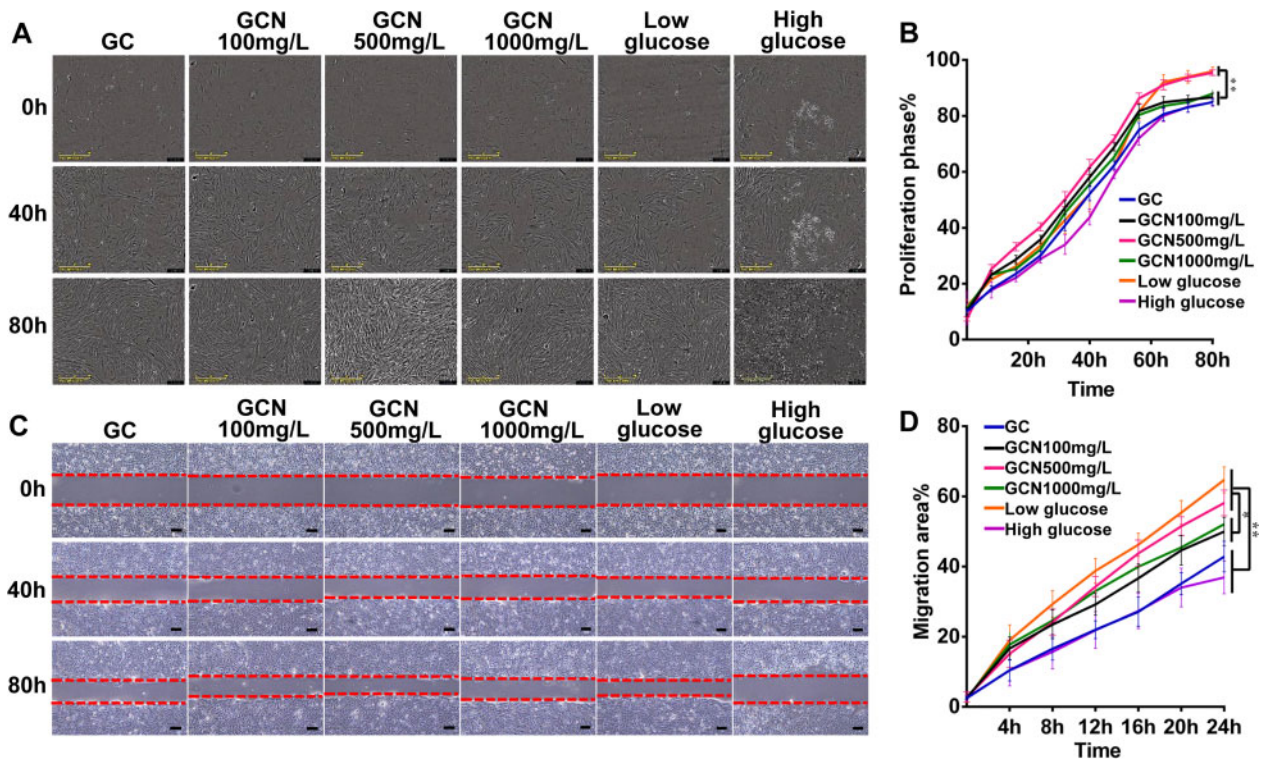


**Figure 2.** In vitro cell biocompatibility of GO-COL-NAC hybrid scaffolds. (A) Images of cell proliferation assay of the NIH 3T3 fibroblasts cultured by extract liquor of different scaffolds at different time-points, observed by the IncuCyte S3 Live-Cell analysis system (scale bars: 200  $\mu$ m). (B) Cell proliferation phase (%) of the NIH 3T3 fibroblasts. (C) Scratch assay experiment images of HaCaT cells cultured by extract liquor of different scaffolds at different time-points, observed under a light microscope (scale bars: 100  $\mu$ m). (D) Migration area (%) of the HaCaT cells at different time-points. (\* $P < 0.05$ , \*\* $P < 0.01$ )

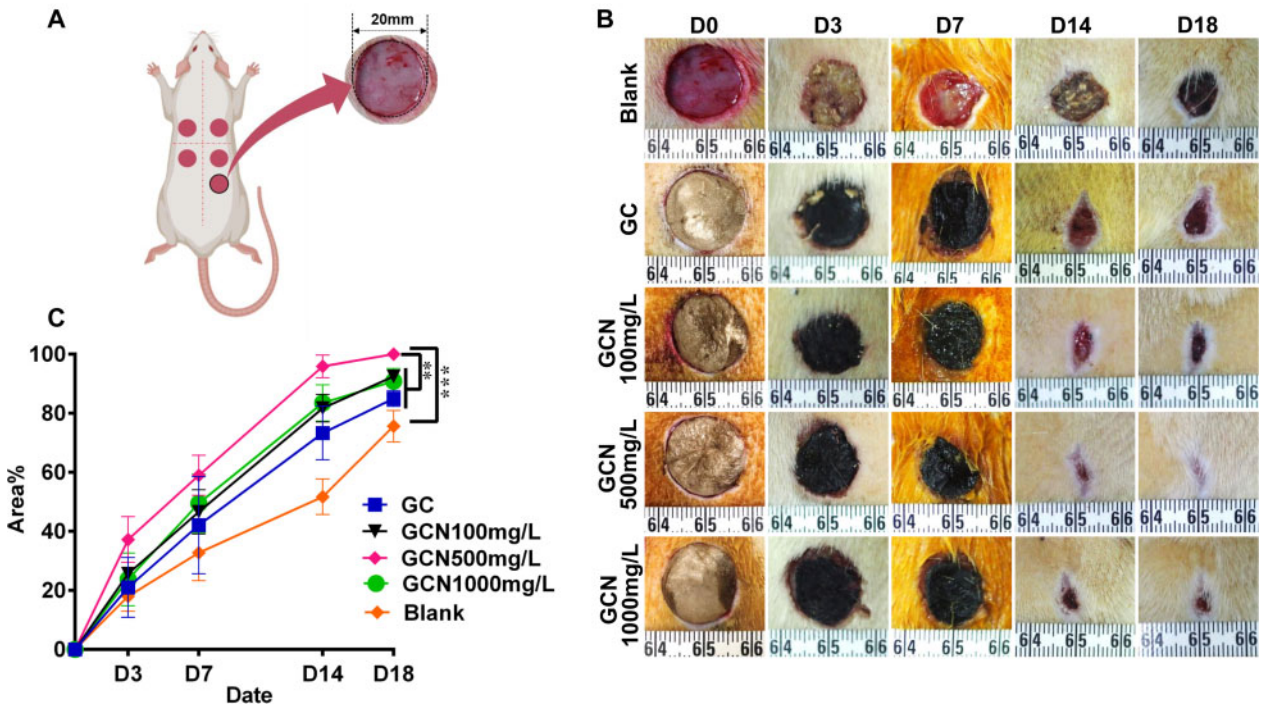


**Figure 3.** The *in vivo* implantation experiments showing that the GO-COL-NAC500 mg/L scaffold possessed the optimal treatment effects across the five groups. (A) Schematic illustration of five 20 mm diameter, full-thickness wounds created at either side of the dorsal Central line. (B) Representative photographs of cutaneous wounds at day 0, 3, 7, 14, 18 post-surgery. GO-COL-NAC500 mg/L group has completely healed at day 18 post-surgery, while other groups have not. (C) Wound closure rates were shown at days 3, 7, 14, 18 post-surgery. (mean  $\pm$  SD; \*\*\* $P < 0.001$ , \*\* $P < 0.01$ ,  $n = 8$  per group)

Fig. 3C further reveals this trend. On the 18th day, all the wounds treated by the GCN500 mg/L scaffolds presented an almost complete wound closure (100%), remarkably faster than that of group GC ( $84.97 \pm 1.01\%$ ), group GCN100 mg/L ( $92.54 \pm 0.77\%$ ) and group GCN1000 mg/L ( $90.86 \pm 1.77\%$ ), while the healing rate of the blank control was only  $75.63 \pm 2.18\%$  at the lowest ( $P < 0.05$ ).

HE staining of wound tissue 18 days after surgery was shown in Fig. 4A. The scaffolds implanted were fully absorbed; however, its outline was indistinguishable. The newly generated skin tissue was found in the defect areas. However, the blank control group still presented remarkable tissue defects, where microstructure was disordered and inflammatory cell was infiltrated. The wound treated by GCN500 mg/L scaffolds had been repaired almost completely with the continuous epidermis, whereas the other groups resulted in defect healing with discontinuous epidermis. Masson's Trichrome staining (Fig. 4B) evaluating the collagen deposition demonstrated that the GCN500 mg/L scaffold could better repair the diabetic wound, which exhibited a uniform and thick collagen bundle deposition compared to other groups. Figure 4C was plotted for comparison of the remaining wound length in different groups. The unhealed wound length for GCN500 mg/L ( $1568 \pm 164.2 \mu\text{m}$ ) was shorter than that of GC ( $4258 \pm 165.9 \mu\text{m}$ ), GCN100 mg/L ( $3229 \pm 191.4 \mu\text{m}$ ), GCN1000 mg/L ( $2487 \pm 188.2 \mu\text{m}$ ) and blank control ( $5584 \pm 179.8 \mu\text{m}$ ). Figure 4D was plotted to assess the thickness of the epidermis. The GCN500 mg/L treated group appeared the best epidermal maturation with uniform thickness ( $80.81 \pm 2.36 \mu\text{m}$ ), while blank control and GC group appeared with incomplete epithelization. The thickness of the GCN100 mg/L and GCN1000 mg/L were  $116.9 \pm 2.36 \mu\text{m}$  and  $121.9 \pm 2.48 \mu\text{m}$ , respectively, which was much thicker than the GCN500 mg/L.

CD31 staining (Fig. 5A) was applied to clarify the angiogenesis of the regenerated tissue. The results revealed that the number of blood capillaries in GCN500 mg/L treated group ( $75.42 \pm 3.90$ ) was higher than that of GCN100 mg/L ( $43.75 \pm 2.71$ ), GCN1000 mg/L

( $55.58 \pm 2.35$ ) and blank control ( $26.25 \pm 2.18$ ), which was attributed to the pro-angiogenesis effect of NAC (Fig. 5B).

### Detection of antioxidant stress level

The RT-PCR was conducted to monitor mRNA expression of various antioxidant kinases of the wound skin sample on day 18 post-surgery. The results demonstrated that GCN500 mg/L significantly increased the mRNA levels of CAT, SOD and GPx, (Fig. 6C–E), which meant a stronger anti-oxidative stress ability compared to other scaffolds. This effect may benefit from a more appropriate concentration of NAC loading on the scaffold.

### Discussion

A diabetic wound is a common and tiring complication, leading cause of disability and mortality among diabetics [32]. Biomaterials offer promising potential in the induction of tissue regeneration for chronic wound healing. In this study, we fabricated a conductive GO-functionalized COL hybrid scaffold loaded with NAC for wound healing in diabetic rats. It was demonstrated that the GO-COL scaffolds loading 500 mg/L NAC distinctly induced collagen deposition, re-epithelialization and angiogenesis in the wound sites of diabetic rat model; also, it inhibited inflammation reaction. This non-toxic and biodegradable scaffold took advantage of the inherent advantages of GO and COL in promoting tissue regeneration, which could be synthesized by a simple and feasible procedure. It provided locally and sustainably released NAC in diabetic wounds, avoiding both the side effects of systemic drug use and the repetitiveness of topical application.

Diabetic wounds are characterized by severe oxidative stress and persistent inflammatory response, an important cause for which is the excess production of the ROS [33]. Previous studies revealed the activation of nucleotide-binding and oligomerization domain-like receptor family pyrin domain-containing 3 (NLRP3) inflammasome in DM patients via a ROS-mediated pathway [34], which would

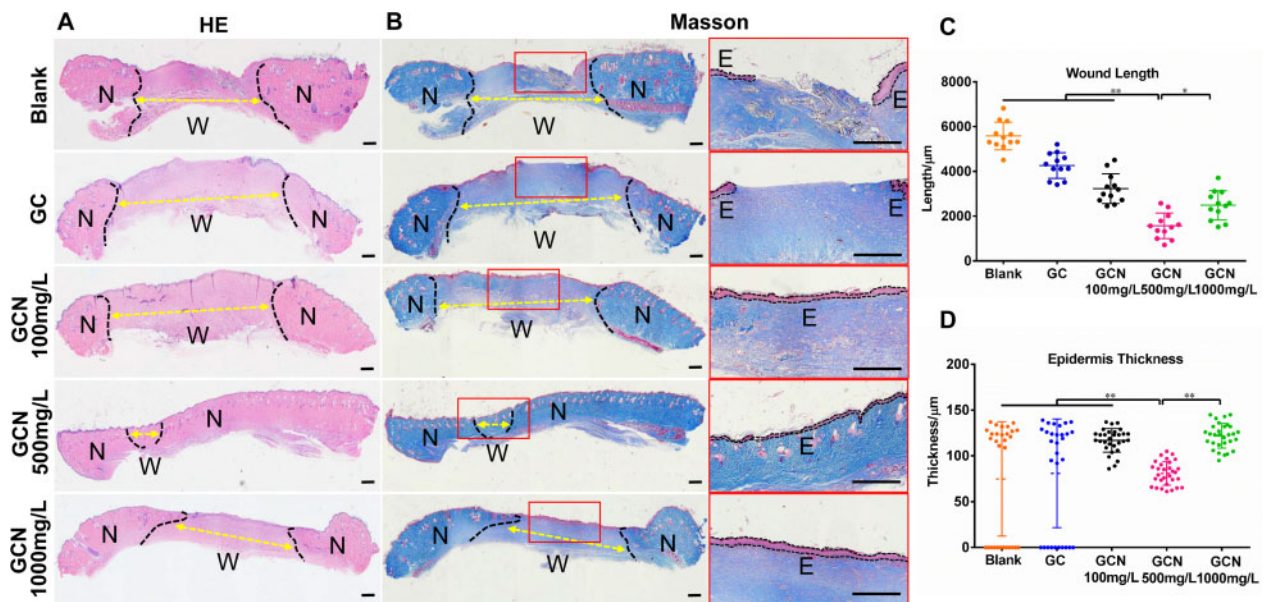


**Figure 4.** Histological analysis revealing better exhibited better repair effect in the GO-COL-NAC500 mg/L group at day 18 post-surgery compared with other groups. (A) H&E staining and (B) Masson staining images of the wound section were presented at day 18 post-surgery. The black dotted line represents the interface between the incomplete wound area and the neo-epidermis, the yellow arrows indicate the remaining wound length. W, remaining wound area; N, neo-epidermis; E, epidermis. Scale bar = 500  $\mu\text{m}$ . (C) Length of the remaining wound and (D) thickness of regenerated epidermal were analyzed (\*\* $P < 0.01$ , \* $P < 0.05$ )

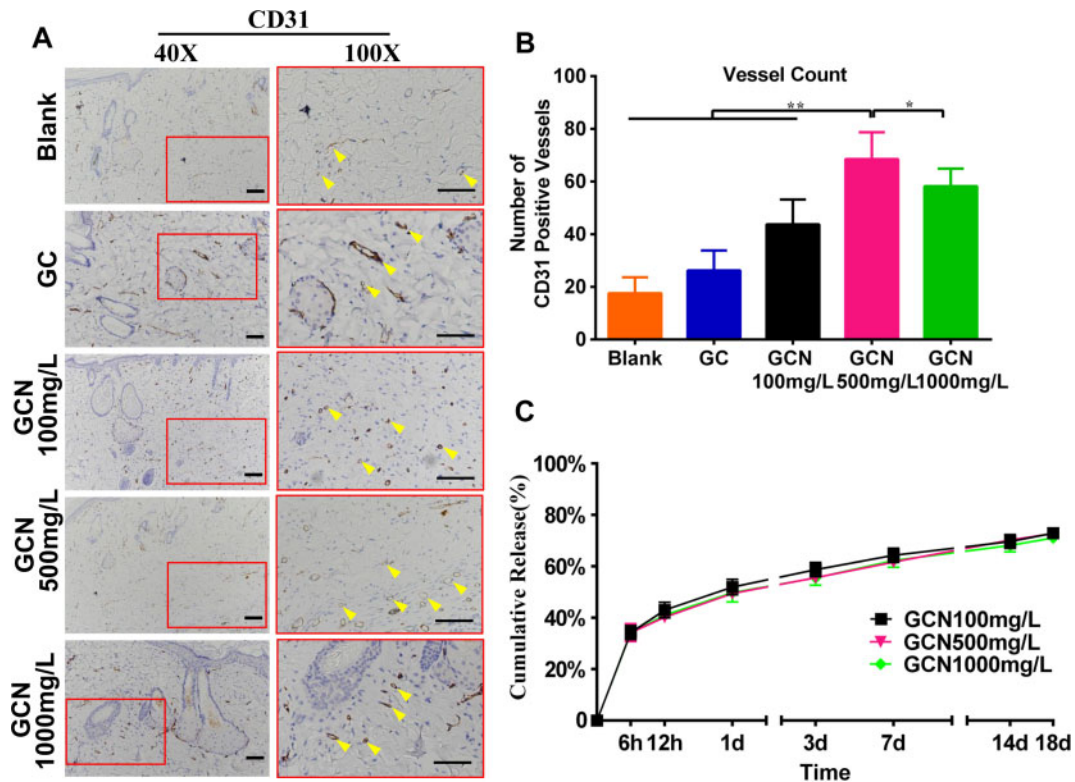


**Figure 5.** (A) Immunohistochemical staining for CD31 of the regenerated skin on day 18 post-surgery showing a significant increase in the number of vessels in the GO-COL-NAC500 mg/L group compared to others. Yellow arrows indicate CD31 positive vascular endothelial cells, Scale bar = 200  $\mu$ m. (B) Quantitative analysis of the number of CD31 positive vessels on the regenerated skin. (\*\*\*)  $P < 0.001$ , (\*\*)  $P < 0.01$ . (C) The drug release curve of the NAC loaded in GO-COL-NAC scaffolds ( $n = 3$  per sample per time-point). The cumulative NAC release increased rapidly in the first 24 days, but still maintained an upward trend until the 18th day, indicating that the GO-COL-NAC scaffold was capable of sustained drug release

impair wound healing in mice and humans with type 2 diabetes [35]. Pierce *et al.* [36] concluded that excessive ROS causes damages to cellular membranes, proteins, lipids; the DNA is thus deleterious to wound healing. Additionally, ROS was reported to regulate the synthesis and release of various proinflammatory cytokines, including TNF- $\alpha$ , IL-1 $\beta$  by activating transcription factors, including nuclear factor erythroid 2-related factor 2 (Nrf-2) and nuclear factor kappa B (NF- $\kappa$ B) [37]. In other words, the accumulation of ROS not only participates in the development of diabetic wound but also propagate the inflammatory cascade, which impairs wound healing and hinders the formation of new tissues. Hence, Boniakowski *et al.* [38] declared that therapies that permit regulated and programmed wound inflammation are promising approaches for diabetic management as well as other pathologic wounds.

NAC, a sulfhydryl antioxidant, has been receiving growing research attention in the chronic wound because of its ability to regulate excessive inflammatory response and prevents oxidative stress triggered by ROS [39]. The proven mechanisms of the NAC promoting wound healing are as follows: (i) As a precursor of GSH, NAC increases the synthesis of this antioxidant, which reduces free radical damage. (ii) NAC upregulates the PI3K expression, which is responsible for growth factor and cytokine production necessary for wound healing. (iii) NAC activates the stat3 expression, a protein essential for migration of dermal microvascular endothelial cells to promote angiogenesis. (iv) NAC increases the expression of MMP-1, a protein responsible for ECM formation and re-epithelialization [22, 40]. In the current study, compared with the GC scaffold, GCN500 mg/L scaffold significantly increased the mRNA

expression of antioxidant enzymes (CAT, SOD, GPx) in the wound tissues 18 days after surgery (Fig. 6C and D), which was attributed to the NAC. It meant that GCN500 mg/L scaffold exhibited higher levels of antioxidant stress. Meanwhile, due to the angiogenic effect of the NAC, and the amelioration of the wound micro-environment after free radical scavenging, immunohistochemical examination of the wound tissue of GCN500 mg/L scaffold found that there was more angiogenesis than that of the GC scaffold (Fig. 5A and B). Also, the comparison of the GCN500 mg/L and GC scaffold results *in vitro* cell proliferation, cell migration, and cellular COL mRNA expression was also consistent with the above (Figs. 2 and 6A, B). However, the premise of achieving these results is that the NAC-loaded scaffold can release an effective drug concentration on the wound surface sustainably. Therefore, the release kinetics of the NAC loaded in the GO-COL-NAC scaffolds will be a crucial parameter.

As shown in Fig. 5C, NAC-loaded scaffolds present a rapid drug release in the first 24 h, mainly due to free NAC release deposited within the pores of the scaffolds. And then, until the 18th day, the curve shows a slow upward trend, which may be associated with the breakage of chemical bonds between NAC and the scaffold, causing more NAC to be released slowly.

However, the differences in results between the NAC-loaded scaffolds suggest that NAC concentration plays a crucial role. Tsai *et al.* [22] reported a dose-dependent manner with NAC concentrations of 0.1 mM to 1.0 mM by mice burn model. Furthermore, some previous studies have pointed out the specific recommended doses for NAC in dermatologic conditions [41, 42]. In this present



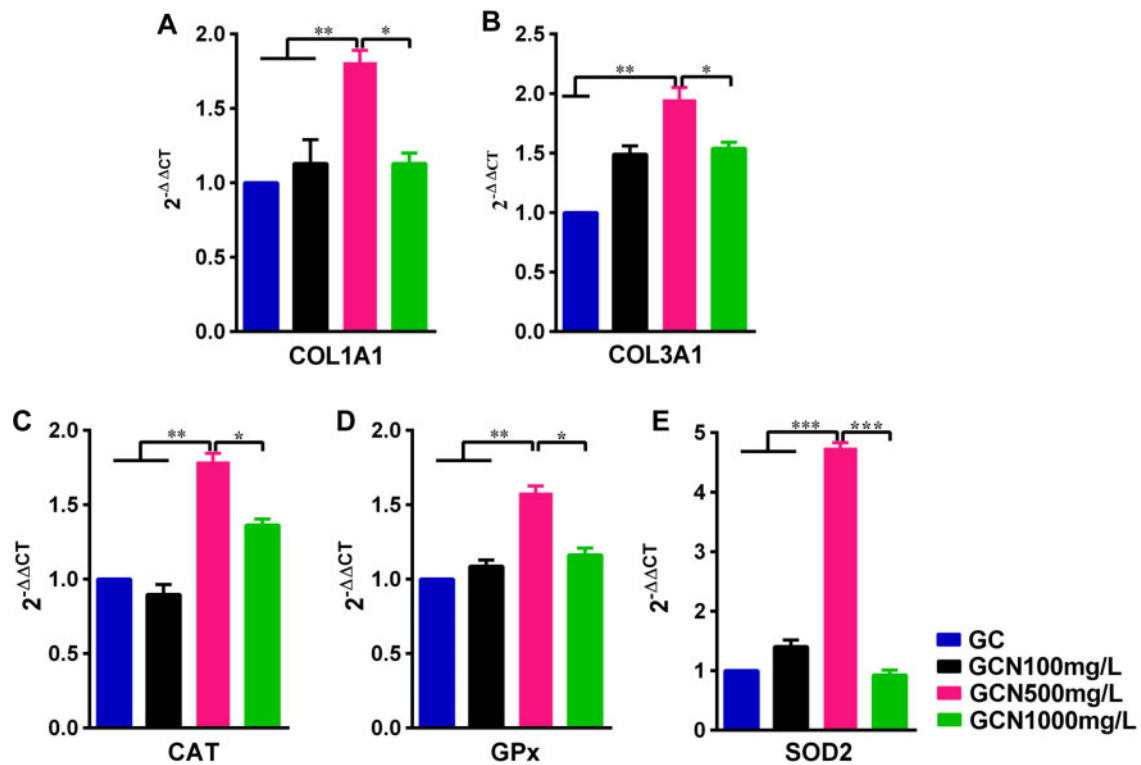


**Figure 6.** Relative mRNA expressions of COL I (A) and COL III (B) of the NIH-3T3 fibroblasts in different extract liquor of the scaffolds. The extract liquor from the GO-COL-NAC500 mg/L scaffold induced significantly higher mRNA expression of the COL I and COL III. (C, D, E) Analysis of antioxidant kinases gene expression (CAT, GPx and SOD2) of the wound skin sample on day 18 post-surgery revealed that the GO-COL-NAC500 mg/L scaffold exhibited stronger anti-oxidative stress ability than the other two groups (\* $P < 0.05$ , \*\* $P < 0.01$ , \*\*\* $P < 0.001$ )

research, compared with the NAC loading concentration of 100 mg/L, the GCN500 mg/L treated wound presented a more uniform and thicker collagen bundle deposition, better epidermal maturation with uniform thickness and more angiogenesis (Figs. 4 and 5A). This may be due to the longer maintenance time of effective drug concentration in the wound caused by the higher NAC concentration in a certain range. Nevertheless, 1000 mg/L NAC loading concentration showed relatively poor results in the experiment compared with 500 mg/L, which implies the loading range due to excessive drug concentration. Tsai *et al.* [22] confirmed that the expression of MMP-1 was positively regulated by NAC drugs, and the production of excessive MMP-1 would lead to excessive epidermal hyperplasia, which explained the thickest epidermis in the highest NAC loading group (1000 mg/L) (Fig. 4B). The optimal dose of NAC in topical administration of diabetic wound healing still remains inconclusive; the related research needs to be further carried out.

Additionally, an ideal scaffold using for wound healing should also be endowed with high water absorption and retention capacity, and porosity. Both COL and GO have been shown to have rich hydrophilic groups [43, 44], and the engineered scaffolds demonstrated a distinct porous structure, which ensures the good physical properties of the scaffolds (Supplementary Fig. S1). When applied on the wound, on the one hand, the hybrid scaffold can absorb excess exudate from the wound, and maintain a humid micro-environment locally on the wound, thus conducive to the formation of the granulation tissue. On the other hand, its porous structure facilitates the exchange of oxygen and matter between the cells that grow into the scaffold [30]. Moreover, the previously suspected biotoxicity of GO has not been observed in our study, which may be

due to the low concentration of GO in the scaffolds [45], and the modification of COL and NAC to improve its biocompatibility. According to the literature, the toxicity of GO is mainly related to its size, concentration and preparation process, the small-sized and low-concentration GO is usually considered to have good biocompatibility [46].

## Conclusion

In this study, we developed a NAC-loaded GO-COL hybrid scaffold with good biocompatibility and degradability. When the NAC concentration loading on the scaffold is assigned to 500 mg/L, the hybrid scaffold presents a better efficiency to promote diabetic wound healing by resisting oxidative stress, promoting angiogenesis, accelerating ECM-synthesis and facilitating epithelization. This scaffold with valuable therapy potential might enrich the approaches for surgeons in diabetic wound treatment in the future.

## Acknowledgments

The authors wish to appreciate the Analytical & Testing Center of Huazhong University of Science and Technology.

## Supplementary data

Supplementary data are available at REGGIO online.

Conflict of interest statement. None declared.

## Funding

This study received financial support by the National Key R&D Program of China (2019YFA0110500), and the National Natural Science Foundation of China (82020108020, 81873941 and 81701922).

## References

- Patel S, Srivastava S, Singh MR *et al.* Mechanistic insight into diabetic wounds: pathogenesis, molecular targets and treatment strategies to pace wound healing. *Biomed Pharmacother* 2019;112:108615.
- Vijayakumar V, Samal SK, Mohanty S *et al.* Recent advancements in biopolymer and metal nanoparticle-based materials in diabetic wound healing management. *Int J Biol Macromol* 2019;122:137–48.
- Soares RDF, Campos MGN, Ribeiro GP *et al.* Development of a chitosan hydrogel containing flavonoids extracted from *Passiflora edulis* leaves and the evaluation of its antioxidant and wound healing properties for the treatment of skin lesions in diabetic mice. *J Biomed Mater Res* 2020;108:654–62.
- Senturk B, Demircan BM, Ozkan AD *et al.* Diabetic wound regeneration using heparin-mimetic peptide amphiphile gel in db/db mice. *Biomater Sci* 2017;5:1293–303.
- Özay Y, Güzel S, Yumrutaş Ö *et al.* Wound healing effect of kaempferol in diabetic and nondiabetic rats. *J Surg Res* 2019;233:284–96.
- Hu H, Xu FJ. Rational design and latest advances of polysaccharide-based hydrogels for wound healing. *Biomater Sci* 2020;8:2084–101.
- Li R, Xu Z, Jiang Q *et al.* Characterization and biological evaluation of a novel silver nanoparticle-loaded collagen-chitosan dressing. *Regen Biomater* 2020;7:371–80.
- Levingstone TJ, Ramesh A, Brady RT *et al.* Cell-free multi-layered collagen-based scaffolds demonstrate layer specific regeneration of functional osteochondral tissue in caprine joints. *Biomaterials* 2016;87:69–81.
- Zeng Y, Zhou M, Mou S *et al.* Sustained delivery of alendronate by engineered collagen scaffold for the repair of osteoporotic bone defects and resistance to bone loss. *J Biomed Mater Res* 2020;108:2460–72.
- Cholas R, Kunjalukkal Padmanabhan S, Gervaso F *et al.* Scaffolds for bone regeneration made of hydroxyapatite microspheres in a collagen matrix. *Mater Sci Eng C Mater Biol Appl* 2016;63:499–505.
- Belaid H, Nagarajan S, Teyssier C *et al.* Development of new biocompatible 3D printed graphene oxide-based scaffolds. *Mater Sci Eng C Mater Biol Appl* 2020;110:110595.
- Ge S, Xi Y, Du R *et al.* Inhibition of in-stent restenosis after graphene oxide double-layer drug coating with good biocompatibility. *Regen Biomater* 2019;6:299–309.
- Shin SR, Aghaei-Ghareh-Bolagh B, Dang TT *et al.* Cell-laden microengineered and mechanically tunable hybrid hydrogels of gelatin and graphene oxide. *Adv Mater* 2013;25:6385–91.
- Shi X, Chang H, Chen S *et al.* Regulating cellular behavior on few-layer reduced graphene oxide films with well-controlled reduction states. *Adv Funct Mater* 2012;22:751–9.
- Baradaran S, Moghaddam E, Basirun WJ *et al.* Mechanical properties and biomedical applications of a nanotube hydroxyapatite-reduced graphene oxide composite. *Carbon* 2014;69:32–45.
- Kurapati R, Russier J, Squillaci MA *et al.* Dispersibility-dependent biodegradation of graphene oxide by myeloperoxidase. *Small* 2015;11:3985–94.
- Choe G, Oh S, Seok JM *et al.* Graphene oxide/alginate composites as novel bioinks for three-dimensional mesenchymal stem cell printing and bone regeneration applications. *Nanoscale* 2019;11:23275–85.
- Ansari FA, Mahmood R. Carnosine and N-acetyl cysteine protect against sodium nitrite-induced oxidative stress in rat blood. *Cell Biol Int* 2018;42:281–93.
- AlMatar M, Batool T, Makky EA. Therapeutic potential of N-acetylcysteine for Wound healing, acute bronchiolitis, and congenital heart defects. *Curr Drug Metab* 2016;17:156–67.
- Ozkaya H, Omma T, Bag YM *et al.* Topical and systemic effects of N-acetyl cysteine on wound healing in a diabetic rat model. *Wounds* 2019;31:91–6.
- Zayed MA, Wei X, Park K-M *et al.* N-acetylcysteine accelerates amputation stump healing in the setting of diabetes. *FASEB J* 2017;31:2686–95.
- Tsai M-L, Huang H-P, Hsu J-D *et al.* Topical N-acetylcysteine accelerates wound healing in vitro and in vivo via the PKC/Stat3 pathway. *Int J Mol Sci* 2014;15:7563–78.
- Hou J, Chen L, Zhou M *et al.* Multi-layered polyamide/collagen scaffolds with topical sustained release of N-acetylcysteine for promoting wound healing. *Int J Nanomedicine* 2020;15:1349–61.
- Zeng Y, Zhou M, Chen L *et al.* Alendronate loaded graphene oxide functionalized collagen sponge for the dual effects of osteogenesis and anti-osteoclastogenesis in osteoporotic rats. *Bioact Mater* 2020;5:859–70.
- Jiang L, Li Y, Xiong C *et al.* Preparation and properties of bamboo fiber/nano-hydroxyapatite/poly(lactic-co-glycolic) composite scaffold for bone tissue engineering. *ACS Appl Mater Interfaces* 2017;9:4890–7.
- Vukosavljevic B, Murgia X, Schwarzkopf K *et al.* Tracing molecular and structural changes upon mucolysis with N-acetyl cysteine in human airway mucus. *Int J Pharm* 2017;533:373–6.
- Zhang Q, Oh JH, Park CH *et al.* Effects of dimethylxalylglycine-embedded poly( $\epsilon$ -caprolactone) fiber meshes on wound healing in diabetic rats. *ACS Appl Mater Interfaces* 2017;9:7950–63.
- Sharma PK, Singh Y. Glyoxylic hydrazone linkage-based PEG hydrogels for covalent entrapment and controlled delivery of doxorubicin. *Biomacromolecules* 2019;20:2174–84.
- Yan Z, Wang W, Wu Y *et al.* Zinc oxide nanoparticle-induced atherosclerotic alterations in vitro and in vivo. *Int J Nanomedicine* 2017;12:4433–42.
- Sumayya AS, Muraleedhara Kurup G. Marine macromolecules cross-linked hydrogel scaffolds as physiochemically and biologically favorable entities for tissue engineering applications. *J Biomater Sci Polym Ed* 2017;28:807–25.
- Liu S, Mou S, Zhou C *et al.* Off-the-shelf biomimetic graphene oxide-collagen hybrid scaffolds wrapped with osteoinductive extracellular matrix for the repair of cranial defects in rats. *ACS Appl Mater Interfaces* 2018;10:42948–58.
- Boulton AJ, Vileikyte L, Ragnarson-Tennvall G *et al.* The global burden of diabetic foot disease. *Lancet* 2005;366:1719–24.
- Song R, Ren L, Ma H *et al.* Melatonin promotes diabetic wound healing in vitro by regulating keratinocyte activity. *Am J Transl Res* 2016;8:4682–93.
- Feng H, Gu J, Gou F *et al.* High glucose and lipopolysaccharide prime NLRP3 inflammasome via ROS/TXNIP pathway in mesangial cells. *J Diabetes Res* 2016;2016:1–11.
- Mirza RE, Fang MM, Weinheimer-Haus EM *et al.* Sustained inflammatory activity in macrophages impairs wound healing in type 2 diabetic humans and mice. *Diabetes* 2014;63:1103–14.
- Pierce GF. Inflammation in nonhealing diabetic wounds: the space-time continuum does matter. *Am J Pathol* 2001;159:399–403.
- Forrester SJ, Kikuchi DS, Hernandez MS *et al.* Reactive oxygen species in metabolic and inflammatory signaling. *Circ Res* 2018;122:877–902.
- Boniakowski AE, Kimball AS, Jacobs BN *et al.* Macrophage-mediated inflammation in normal and diabetic wound healing. *J Immunol* 2017;199:17–24.
- Mehrabi Azar Y, Green R, Niesler CU *et al.* Antioxidant preconditioning improves the paracrine responsiveness of mouse bone marrow mesenchymal stem cells to diabetic wound fluid. *Stem Cells Dev* 2018;27:1646–57.
- Janeczek M, Moy L, Riopelle A *et al.* The potential uses of N-acetylcysteine in dermatology: a review. *J Clin Aesthet Dermatol* 2019;12:20–6.
- Grant JE, Chamberlain SR, Redden SA *et al.* N-acetylcysteine in the treatment of excoriation disorder: a randomized clinical trial. *JAMA Psychiatry* 2016;73:490–6.
- Nakai K, Yoneda K, Murakami Y *et al.* Effects of topical N-acetylcysteine on skin hydration/transepidermal water loss in healthy volunteers and atopic dermatitis patients. *Ann Dermatol* 2015;27:450–1.

- 
43. Shekhter AB, Fayzullin AL, Vukolova MN *et al.* Medical applications of collagen and collagen-based materials. *Curr Med Chem* 2019;26:506–16.
  44. Kumar S, Wani MY, Arranja CT *et al.* Synthesis, physicochemical and optical properties of bis-thiosemicarbazone functionalized graphene oxide. *Spectrochim Acta A Mol Biomol Spectrosc* 2018;188:183–8.
  45. Liao C, Li Y, Tjong SC. Graphene nanomaterials: synthesis, biocompatibility, and cytotoxicity. *Int J Mol Sci* 2018;19:3564.
  46. Zhang H, Peng C, Yang J *et al.* Uniform ultrasmall graphene oxide nanosheets with low cytotoxicity and high cellular uptake. *ACS Appl Mater Interfaces* 2013;5:1761–7.